Dedicated to innovation in aerospace

NLR-TP-2022-244 | December 2022

Thermal and Structural Modelling of Thermoset Composite Repairs Towards Optimization of the Cure Cycle for Minimum Distortion

CUSTOMER: NLR

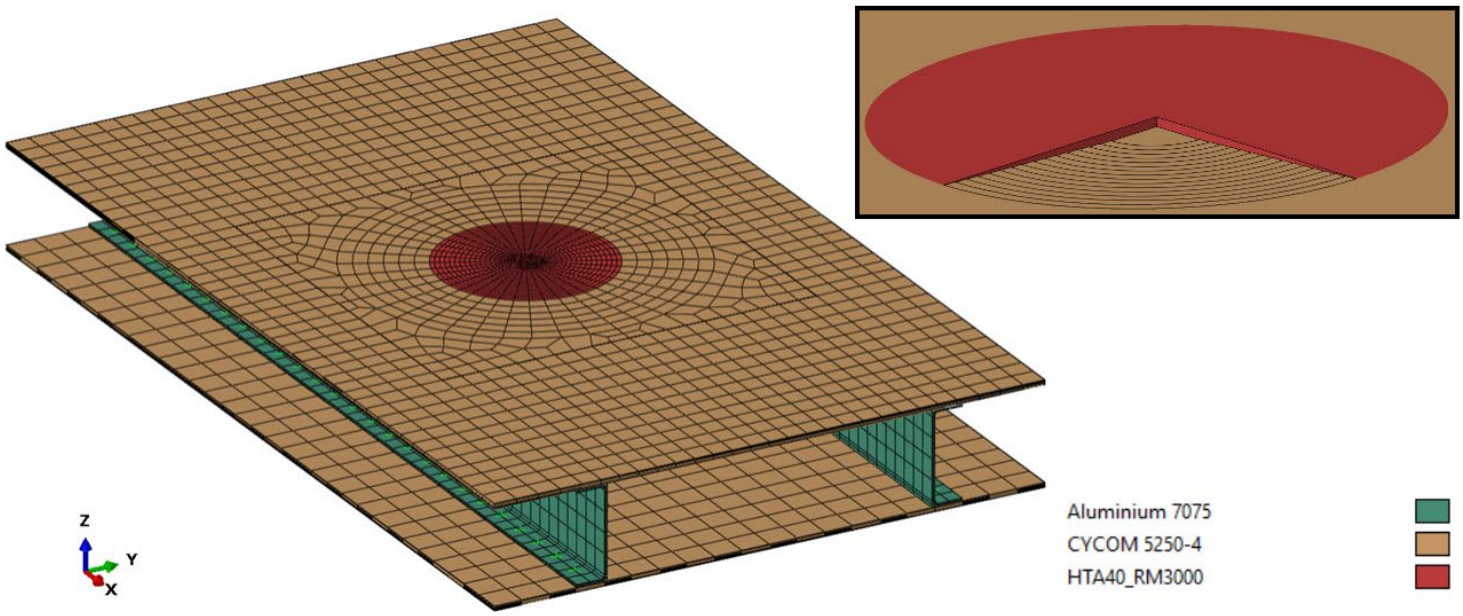

Royal NLR - Netherlands Aerospace Centre

Dedicated to innovation in aerospace

Thermal and Structural Modelling of Thermoset Composite Repairs Towards Optimization of the Cure Cycle for Minimum Distortion

Problem area

During manufacturing of composite materials residual stresses can result in distortion of the final product. In aerospace manufacturing the use of shimming caused by part distortions during assembly should be minimized. This is especially critical when building on existing parts, e.g. for a repair, as the added material has to conform to the original structure. Furthermore, the underlying structures, such as aluminium spars in a wingbox section, can strongly influence the repair quality. For example by excessive extraction of heat required to cure the repair patch.
To predict temperature distributions, the amount of residual stress and distortion during and after a composite repair numerical modelling of the process can be employed. The model can subsequently be used to inform the mechanic on possible problems with the repair before it is performed. Furthermore, modelling approaches can be used to optimize the repair process to obtain high quality repairs without extensive experimental work.

Description of work

In this study a numerical model is developed to predict residual stress and strain during the cure of an advanced Bismaleimide (BMI) resin. To this end, the cure kinetics of the BMI resin RM3000 have been characterized using DSC measurements. UD and twill weave properties are determined by homogenization techniques, where the matrix stiffness is evaluated using the Cure-Hardening Instantaneously Linear Elastic (CHILE) model depending on the degree of cure. The cure model is implemented both in a MATLAB routine and in ABAQUS subroutines. In the MATLAB routine, a single point is quickly evaluated to obtain residual stress and strain after cure for a given temperature cycle. This fast analysis allows for optimization of the process, which in this study is performed by optimizing the temperature cycle for minimum strain after cure. The ABAQUS subroutines are used to evaluate whole laminates and more complex structures where the repair patch is incorporated in the model. In a subsequent thermal-mechanical model, both the temperature distribution as well as the residual stress and strain after cure have been obtained. Additionally, the more computationally expensive ABAQUS implementation is used to analyse the effectiveness of the optimized cure cycle.

REPORT NUMBER
NLR-TP-2022-244

AUTHOR(S)
T.P.A. Koenis
N. van Hoorn
S.M. Moghadasi

REPORT CLASSIFICATION
UNCLASSIFIED

DATE
December 2022

KNOWLEDGE AREA(S)
Computational Mechanics and Simulation Technology
Structures and Manufacturing Technology

DESCRIPTOR(S)
Virtual Manufacturing
Composite Scarf Repair
Numerical Methods
Proces Optimization

Results and conclusions

The optimization using the MATLAB implementation showed a reduction of 19% in strain due to curing of the resin. Further analysis of the best cure cycles and the sensitivity of the strain to different cure cycle parameters shows that a long first dwell is most important in the reduction of these strains. This effect is strongly dependent on the characterized cure kinetics which makes it difficult to repeat exactly in an experimental setting. However insights gained by this optimization are of value for further experimental work.
The effect of the optimized cure has first been analysed for a simple scarf repair of a laminate using the ABAQUS implementation. It is validated that this optimized cure also results in significantly lower strains for the repair.
Finally, the ABAQUS repair simulation framework is applied to the repair of a composite skin in a wingbox structure. It is observed that the curing of the repair patch results in increased stresses and strains, especially located at the bond between the repair patch and the parent material as well as near the rivet connections between the skin and the spars. Again it has been shown that the optimized cure cycle significantly reduces these strains and residual stresses.

Applicability

It is shown that this framework with optimization of the cure cycle can support the patch fabrication with accurate design and analysis for repairs with minimum distortion. Fast optimization methods are possible, which can subsequently be checked more extensively for components or whole structures. However, further experimental validation of the modelling approach is required.

GENERAL NOTE
This report is based on a presentation held at the ECCOMAS 2022 conference in Oslo, June 5-9, 2022.

Royal NLR
Anthony Fokkerweg 2
1059 CM Amsterdam, The Netherlands
p) +31 88 511 3113
e) info@nlr.nl i) www.nlr.nl

Dedicated to innovation in aerospace

NLR-TP-2022-244 | December 2022

Thermal and Structural Modelling of Thermoset Composite Repairs Towards Optimization of the Cure Cycle for Minimum Distortion

CUSTOMER: NLR

AUTHOR(S):

T.P.A. Koenis	NLR
N. van Hoorn	NLR
S.M. Moghadasi	NLR

Royal NLR - Netherlands Aerospace Centre

This report is based on a presentation held at the ECCOMAS 2022 conference in Oslo, June 5-9, 2022.

CUSTOMER	**NLR**
CONTRACT NUMBER	**---**
OWNER	**NLR**
DIVISION NLR	**Aerospace Vehicles**
DISTRIBUTION	**Unlimited**
CLASSIFICATION OF TITLE	**UNCLASSIFIED**

APPROVED BY:		**Date**
AUTHOR	T.P.A. Koenis	14-12-2022
REVIEWER	R.J.C. Creemers	14-12-2022
MANAGING DEPARTMENT	A.A. ten Dam	15-12-2022

Summary

During manufacturing of composite materials residual stresses can result in distortion of the final part. This distortion is even more critical when building on existing parts, such as for a repair, as the added material has to conform to the original structure. To predict this distortion due to curing of thermoset carbon-matrix composite repairs, a numerical modelling method is employed. It has been observed that the temperature cycle applied for the cure of thermoset composites can significantly influence the amount of residual stress and resulting deformation after manufacturing. Therefore, a method is devised to parametrise and subsequently optimize this temperature cycle for minimum distortion after manufacturing. Numerical tests with the optimised temperature cycle resulted in a 36% reduction in process induced strain for a repair of a flat laminate plate. The same methodology is demonstrated on a more complex wingbox structure consisting of two composite skins connected by two C-spars where a scarf repair is applied in the skin. The repair patch is locally heated by a heating blanket to cure the repair patch. A subsequent thermal-mechanical model is used to investigate the amount of residual stress and strain after cure and the influence of underlying structural elements on the repair. The developed framework can support the patch fabrication with accurate design and analysis for repairs with minimum distortion. Which in turn will result in development of more cost-effective composite repairs.

Contents

1 Introduction

The use of Carbon Fibre Reinforced Polymer (CFRP) materials in aircraft structures is increasing significantly and advanced manufacturing capabilities are required to accomplish efficient and effective use of these materials. The production process can be optimised by numerical process simulation (i.e., virtual manufacturing). For instance, to minimise the residual stresses to ensure a first-time-right composite part.

Process simulation is a topic that has been extensively researched. Specifically on the composite curing process numerous PhD researches have been conducted. Johnston [1] investigated process-induced deformation for autoclave processing and defined the CHILE approach. Wijskamp, Svanberg, and Garstka [2, 3, 4] investigated process induced distortions to allow for high-precision composite manufacturing. Similarly, Nielson focussed on larger parts for wind turbines [5]. Their approaches show similarities and these methods have been implemented by several other authors to assess the sensitivities of input parameters [6, 7]. Their approaches have mainly been applied to generic composite parts. However, it has become imperative to also focus on structural repairs of composite parts. A successful repair can prevent replacement of a part and reduce the cost and downtime. Beside structural assessment of composite repairs [8, 9] the literature on process simulation of composite repairs is limited [10, 11]. Additionally, as composites in aerospace become more advanced, obtaining sufficient material data for accurate modelling can be a challenging and expensive process [12]. One example are Bismaleimide (BMI) resins that are used for high temperature applications [13, 14].

The goal of this paper is to predict residual stresses due to curing for repair applications with a HTA40/RM3000 BMI material and investigate optimization possibilities using the modelling framework. In Section 2, the modelling methods and implementations are discussed. In Section 3, the developed cure model is employed to optimize a two hold-stage cure cycle for minimal formation of residual stress. This optimized cure cycle is first applied to a repair of a flat laminate plate. Finally, in Section 4 this methodology will be applied to model a scarf repair of a generic wing box, modelling laminate skins and aluminium substructures.

2 Cure Modelling Method

In this study, the resin cure is modelled using a calibrated cure kinetics model in combination with the Cure Hardening Instantaneously Linear Elastic (CHILE) model. This is extensively discussed in previous research, and therefore will only be shortly discussed in this paper [12]. The initial implementation of the model is performed in a MATLAB routine to evaluate the degree of cure and developed strains and stresses in a single point.

2.1 Modelling Method

To characterize the RM3000 resin isothermal and dynamic Differential Scanning Calorimeter (DSC) measurements have been performed using a TA instruments Q2000 DSC equipped with a Tzero pan. To describe the cure kinetics of the RM3000 resin system, the autocatalytic Kamal-Sourour model was found to be adequate. The Kamal-Sourour model describes the cure rate as

$$\frac{d\alpha}{dt} = (k_1 + k_2\alpha^m)(1-\alpha)^n \quad (1)$$

with m and n as material constants, α the degree of cure, and k_1 and k_2 as rate constants defined as

$$k_i = A_i e^{\left(\frac{-E_i}{RT}\right)} \; with \; i = 1,2 \quad (2)$$

with A_i the pre-exponential constant, E_i the activation energy, R the universal gas constant, and T the absolute temperature [13]. A non-linear regression method in MATLAB fits the Kamal-Sourour model parameters, A_i, E_i, m and n to the obtained experimental DSC data [12]. The glass transition temperature is defined by the Di Benedetto relation as a function of the degree of cure [14].

$$T_g(\alpha) = T_{g0} + \frac{\lambda\alpha\left(T_{g\infty} - T_{g0}\right)}{1-\alpha(1-\lambda)} \quad (3)$$

Here T_{g0} and $T_{g\infty}$ are the glass transition temperatures at 0% of cure (α=0) and 100% of cure (α=1) respectively and λ a material dependent fitting parameter. These parameters have been calibrated to glass transition temperature measurements using the Optimold cure sensor by Syntesites demonstrated in Pantelelis et al. [15]. The T_g measurements for this calibration were obtained during the cure cycle of a HTA40-RM3000 laminate.

To obtain the degree of cure at gelation (α_{gel}), isothermal DSC experiments have been performed at temperatures of 200, 220, and 240 °C. The method proposed by Gao et al. is employed to determine the degree of cure at gelation from the isothermal DSC measurements [16]. Table 1 displays the Kamal-Sourour parameters as well as the Di Benedetto parameters and degree of cure at gelation as used in this study.

Table 1: Parameters used to characterise the RM3000 BMI resin

Kamal-Sourour parameter	Value	Resin Parameter	Value
A_1 [s^{-1}]	1,605,520	$T_{g\infty}$ [$°C^{-1}$]	233
E_1 [J mol^{-1}]	85,506	T_{g0} [$°C^{-1}$]	15.7
A_2 [s^{-1}]	7,299,464	λ [-]	0.75
E_2 [J mol^{-1}]	85,317	α_{gel} [-]	0.77
n [-]	1.7695		
m [-]	3.3057		

During the curing process the resin transforms from a liquid, to a rubbery like material, and finally to a solid glassy phase. For a correct representation of the resin state an accurate constitutive model is needed. Full viscoelastic models give the closest approximation but require extensive material characterisation [4]. A good alternative is the Cure-Hardening Instantaneously Linear Elastic (CHILE) model by Johnston et al. [1, 17]. This model has been implemented and calibrated for the RM3000 resin in previous work of the authors [12].

The cure dependent resin properties and the fibre properties are homogenised using the Composite Cylinder Assemblage (CCA) model [18, 19] to obtain UD ply properties. To obtain the twill weave ply properties required for the repair the classical laminate theory is employed as demonstrated by Hoorn et al. [20]. To obtain the twill weave homogenized coefficient of thermal expansion (CTE) and chemical shrinkage (CCS) a more elaborate method is employed in the form of the Mosaic model of Ishikawa and Chou [21]. As a result, the full three-dimensional twill weave ply properties can be described as a function of Tg. The complete modelling method is implemented in the EXPAN and USDFLD subroutines in Abaqus, which has been validated for the fully characterized AS4/8852 laminates in previously published research [12].

3 Cure Optimization

A strong advantage of virtual manufacturing simulations is the low cost of process optimization, as no extensive trial and error experimentation is required. To demonstrate some possibilities with the developed cure models, an investigation is performed where the cure models are employed to minimize the amount of deformation occurring due to curing.

3.1 Optimization Method

A two stage hold cure cycle is parametrized to systematically vary the cure cycle and easily evaluate different cure cycles. Figure 1 displays the original two hold cure cycle used for HTA40/RM3000 laminates, where the temperature profile can be fully described using nine parameters. From these parameters, T1 and T4 are fixed, as T1 is the injection temperature and T4 the ambient temperature.
Of the nine variables describing the cure cycle, seven are varied in the optimization. The dwell times (d1 and d2) and heat-up rates (r1, r2 and r3) range from 10-200% of the original value. The upper and lower bound of the first dwell temperature (T2) are 135 and 155 °C and of the second dwell temperature (T3) 185 and 200 °C. Using the Saltelli sampling sequence combinations, the seven input parameters (D) are generated as input [22]. Per parameter an interval (N) of 10,000 is used, resulting in $2N(D+1) = 160{,}000$ sampled cure cycles.
Due to the large number of variables, an analysis with the Abaqus implementation will not be possible within an acceptable time frame. Therefore, the MATLAB implementation is chosen for initial optimization of the cure cycle. As only a single point is evaluated, no computationally expensive Finite Element Analysis (FEA) is required. This reduces the single analysis from 15 minutes to 0.05 seconds, making it possible to evaluate all cure cycles in just over two hours. Per evaluated cure cycle, the process induced thermal and chemical strain, the degree of cure, and total manufacturing time is determined. Besides minimizing for process induced strain, the degree of cure after manufacturing should be sufficiently high. Furthermore, the total manufacturing should not be extremely long and cumbersome to implement in practice.

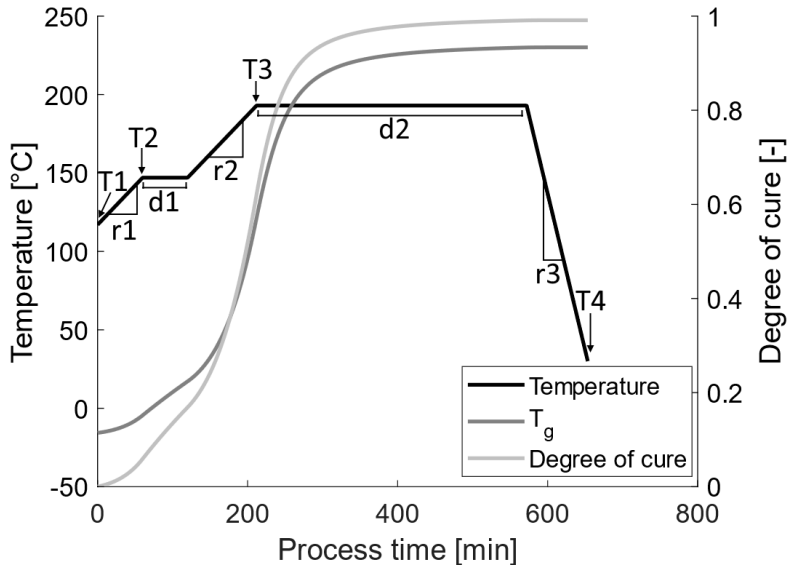

Figure 1: The nine parameters that describe the original cure cycle applied to the composite repairs

3.2 Optimal Cure Cycle

When the MATLAB routine is finished the results are analysed using the Sobol method to obtain the sensitivity of the degree of cure and total strain to the 7 parameters describing the cure cycle [23]. These sensitivities are used to gain insight in the process. An overview of the sensitivities is displayed in Figure 2. It is observed that the degree of cure is largely influenced by the duration of the second dwell (T3). However, the process induced deformation is mainly influenced by the duration of the first dwell combined with effects of other parameters.

Subsequently, the results of the analysis can be employed to extract an optimal cure cycle. From each of the 160,000 evaluated cure cycles the total strain after manufacturing is known. By selecting the cure cycle which results in the lowest strain, a near optimum cure cycle within the given bounds is found. A feasible cure cycle is ensured by constraining the final degree of cure and total manufacturing time. Only cure cycles resulting in a degree of cure larger than 95% and with a manufacturing time less than 16 hours are included. Furthermore, cure cycles with temperature ramps larger than 2 °C/min are excluded as these ramps might not be feasible with the current cure set-up.

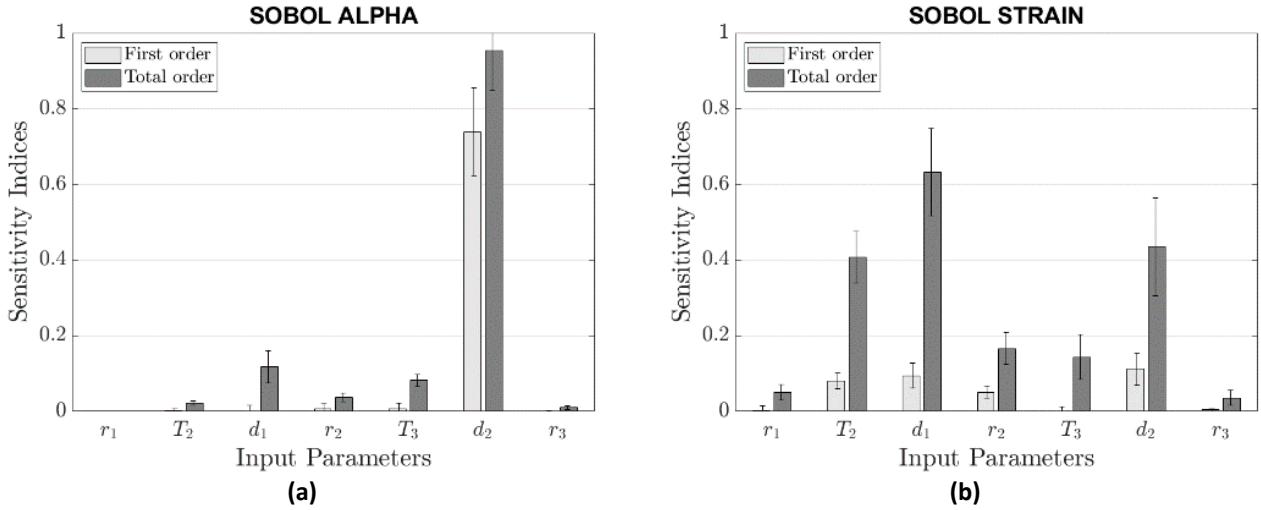

Figure 2: First order Sobol indices and total-effect indices indicating the sensitivity of the seven parameters describing the cure cycle for (a) the degree of cure and (b) the process induced strain

The cure cycle resulting in the least strain after manufacturing is displayed in Figure 3. The most remarkable feature of this cure cycle is the lengthy first dwell, and relatively short second dwell. Analysis of the 50 cure cycles with the lowest strain shows that the best cure cycles reach the gelation point ($\alpha = 0.77$) moments before the end of the first dwell. As soon as the gelation point is reached strains begin to develop, see Figure 3 (a) and (b). By placing the second temperature ramp directly after gelation the chemical shrinkage mostly cancels out the thermal expansion. The optimal two hold stage cure cycle can reduce the total developed strain by 19%. It should be noted that these results are influenced by the accuracy of the resin characterisation. In case the degree of cure is predicted inaccurately, the modelled gelation point might shift. This would reduce the effectiveness of the optimized cure cycle.

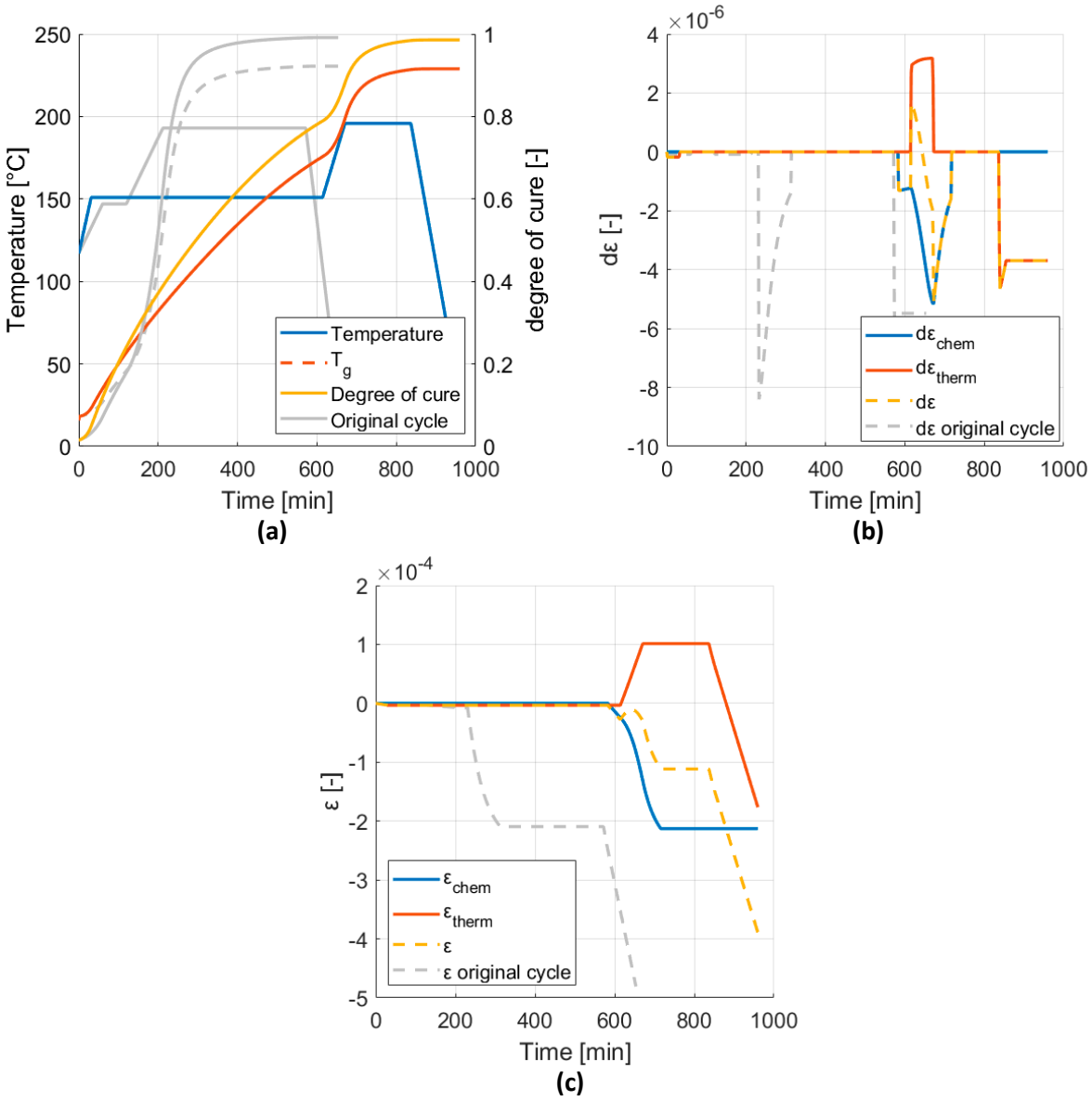

Figure 3: Optimal cure cycle determined for the 160,000 analyzed cycles showing (a) the temperature profile, degree of cure and Tg evolution, (b) the incremental strains and (c) the total strains

3.3 Application of the Optimized Cure Cycle

Abaqus is used to verify that the optimal cure cycle reduces the amount of residual stress in laminate repairs. A Finite Element Analysis (FEA) of a 2.2 mm thick scarf repair in a 300 x 300 x 4.4 mm laminate using the optimized cure cycle is performed. The parent material consists of fully cured IM7-CYCOM 5250-4 UD prepreg material with a $[45,0,-45,90]_{4,s}$ layup with 0.138 mm thick layers. The outline of the scarf repair is removed from the centre of the laminate. The scarf repair consists of 11 layers of 0.2 mm thick twill weave HTA-40 plies with an initial ply size of 33 x 300 mm expanding with 4 mm overlap each ply up to a width of 113 x 300 mm, see Figure 4 (a). Finally, five additional layers are added extending above the parent material. The first four plies overlap with 5 mm and the final ply with 10 mm resulting in a total width increase from 131 to 171 mm over the final 4 plies. The plies of the repair patch are oriented with the same layup as the parent material. It is noted here, that the repair design contains these 5 external (overlap) plies to compensate for the lower stiffness of the repair plies (HTA-fibres) compared to the parent material (IM7-fibres). These extra plies in the repair are necessary to restore the stiffness (and strength) to the same value as for the parent material.

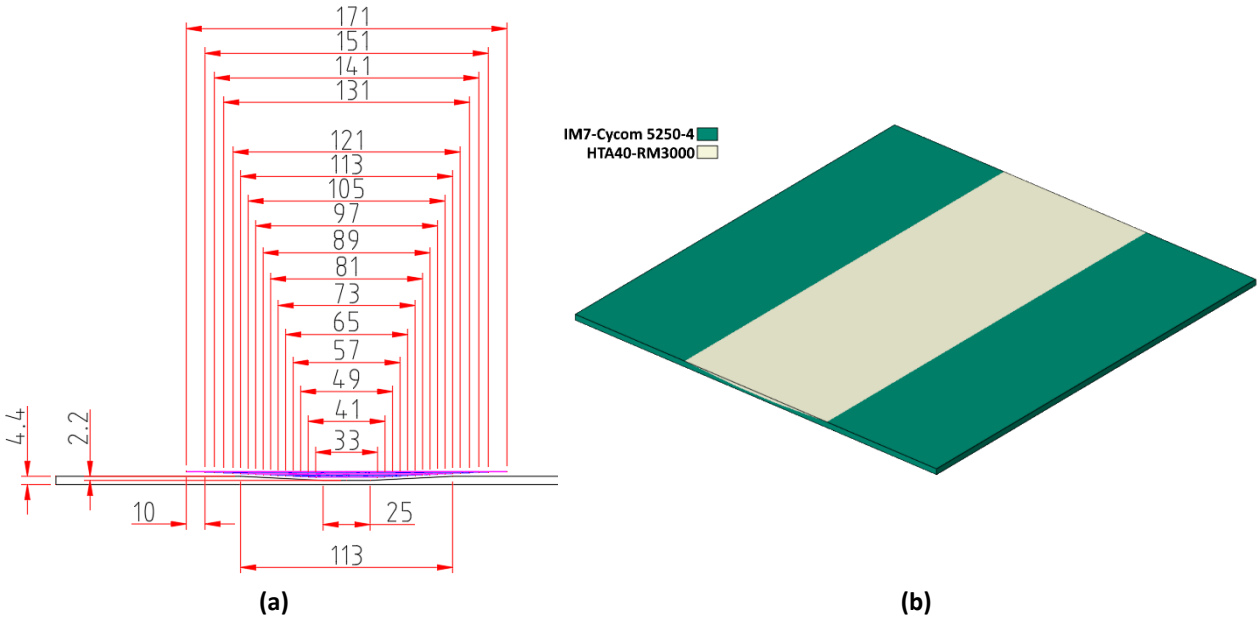

Figure 4: (a) schematic view of the scarf repair including measurements of the geometry removed from the parent material as well as the geometry of the scarf repair patch and (b) the simplified numerical model obtained to represent the scarf repair

The scarf geometry is strongly simplified for the numerical modelling approach. The layer thickness of the repair is assumed equal to the layer thickness of the parent material, t_{ply}=0.138 mm. Therefore, the 16 plies of the scarf repair conform with the parent material, so the repair patch becomes flush and no longer contains any external (overlap) plies as applied in the original design. The reduction of ply thickness in the repair patch does result in a reduction of 30% in structural stiffness of the repair. To restore the lost laminate stiffness, the ply stiffness of the repair material is increased by 30%. Thus the numerical model contains a repair patch is with equal thickness as the parent material, making modelling of the patch much easier, while maintaining the same stiffness as the original design of the repair containing the external overlap plies. Furthermore, a perfect bond between the repair and the parent material is assumed. The laminate is meshed using quadratic hex elements of 10 x 10 mm and a 1 element per ply thickness. The numerical representation of the scarf repair is displayed in Figure 4 (b).

Table 2: Properties of the IM7-CYCOM 5250-4 UD prepreg parent material [24] and the repair resin and fibre parameters [12]

Parent ply properties	**IM7-CYCOM 5250-4**	**Repair resin properties**	**RM3000**	**Repair fibre properties**	**HTA40**
ρ [kg/m^3]	1556	ρ_m [kg/m^3]	1 250	ρ_f [kg/m^3]	1 760
E_{11}[GPa]	162	$E_{m,G}$ [MPa]	3.2e3	$E_{f,11}$ [MPa]	238e3
E_{22}, E_{33}[GPa]	9.51	$E_{m,R}$ [MPa]	3.52	$E_{f,22,33}$ [MPa]	15e3
ν_{12}, ν_{13}, ν_{23}[-]	0.32	$\nu_{m,G}$ [-]	0.365	$\nu_{f,12,13}$ [-]	0.3
G_{12}, G_{13}[GPa]	5.9	$\nu_{m,R}$ [-]	0. 4996	$\nu_{f,23}$ [-]	0.3
G_{23}[GPa]	3.3	$G_{m,G}$ [MPa]	1.17e3	$G_{f,12,13}$ [MPa]	25
CTE_{11}[°C^{-1}]	-1.32 E-6	$G_{m,R}$ [MPa]	1.17	$G_{f,23}$ [MPa]	7
CTE_{22}[°C^{-1}]	30.06 E-6	$CTE_{m,G}$ [°C^{-1}]	4.028E-5	$CTE_{f,11}$[°C^{-1}]	-1E-7
CTE_{33}[°C^{-1}]	0	$CTE_{m,R}$ [°C^{-1}]	3*$CTE_{m,G}$	$CTE_{f,22}$[°C^{-1}]	5.012E-7
		CCS [-]	-0.03252		

During the cure cycle, a homogenous temperature is assumed in the thin laminate [12]. Furthermore, only the scarf repair experiences a change in degree of cure, as the parent material is already cured. The bottom surface of the laminate is pinned, allowing no translations in this surface. After cure, the laminate is released, and fixed at the corners to avoid rigid body motions. The material properties used for the parent and repair materials are displayed in Table 2, with a fibre volume content of 55% in the repair material. The ply stiffness properties after homogenization are increased by 30% to restore the structural stiffness.

Both the original and the optimized cure cycle are applied in the Abaqus model of the simplified scarf repair. Figure 5 displays the results for the max principal and out of plane components of the residual stresses after cure of the repair. The overall residual stresses developed during the original cure cycle are significant but not excessive. However, the residual stress is mainly located at the bond between the repair and the parent material, which is detrimental for the adherence of the repair to the parent material. It is observed that these stresses are mainly in-plane components. The out of plane stress components most likely to cause peeling of the repair are significantly lower. Table 3 gives an overview of stress components with peak tensile and compressive values. It is observed that the peak out of plane normal and shear stresses are just below the 10 MPa for the original cure cycle both in tensile as well as compressive. These out of plane residual stresses are reduced by 21%-27% using the optimized cure cycle.

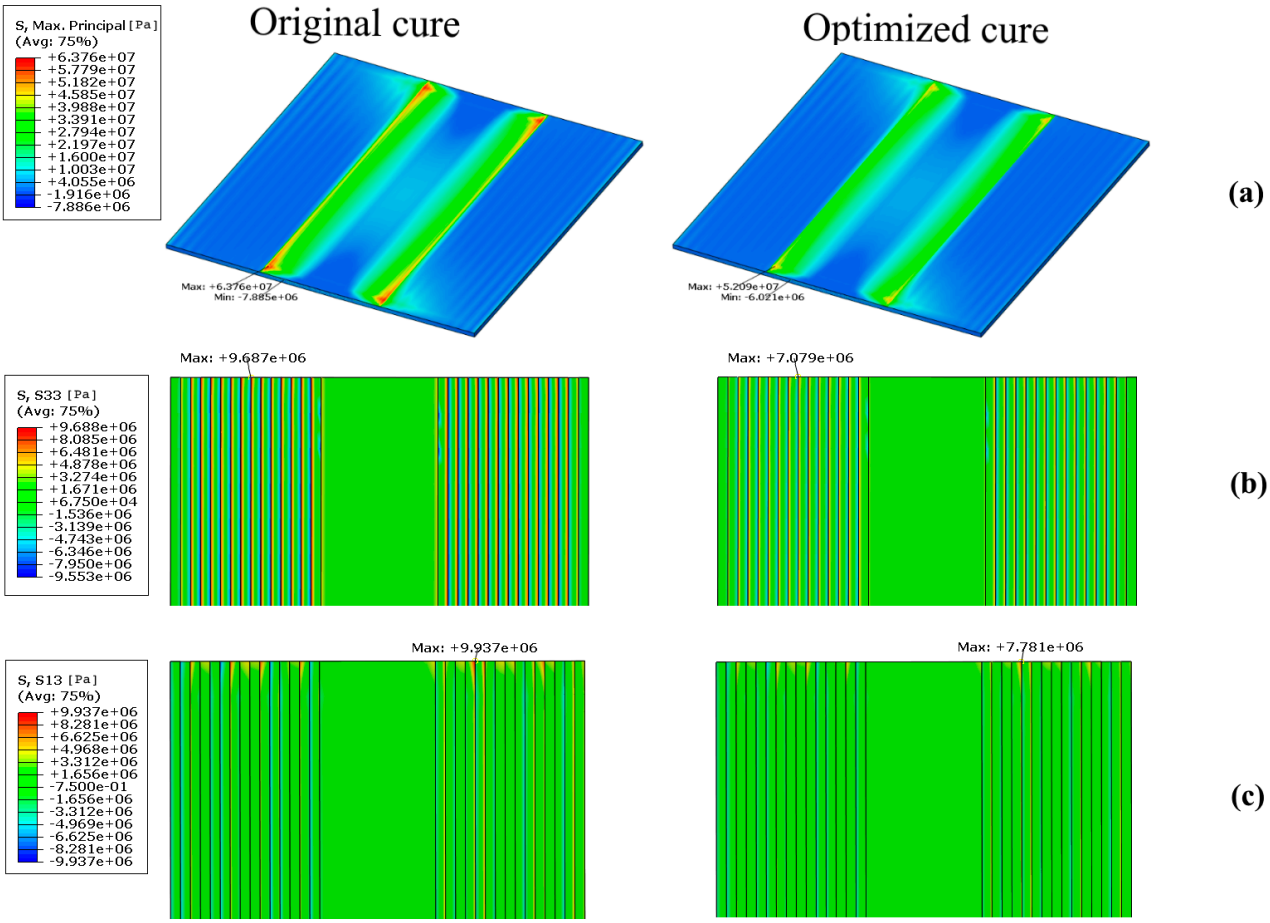

Figure 5: Results of the cure simulation on the twill weave HTA40 RM3000 scarf repair in a 300x300 mm UD IM7-CYCOM-5250-4 laminate using both the original and the optimized cure cycle, displaying results of (a) the max principle stresses, (b) the out of plane normal stress component and (c) the largest component of the out of plane shear stress

Figure 6 displays the strain fields resulting from both the original and the optimized cure cycle. It is observed that similarly to the residual stresses peak tensile strains occur at the interface between the repair and the parent material. This is especially evident in the 90°/y-direction which is perpendicular to the repair orientation. Due to the optimized cure, both the tensile as well as the compressive (shrinkage) strains are reduced by around 19%, corresponding well with the expectations from the optimization routine discussed in Section 3.2.

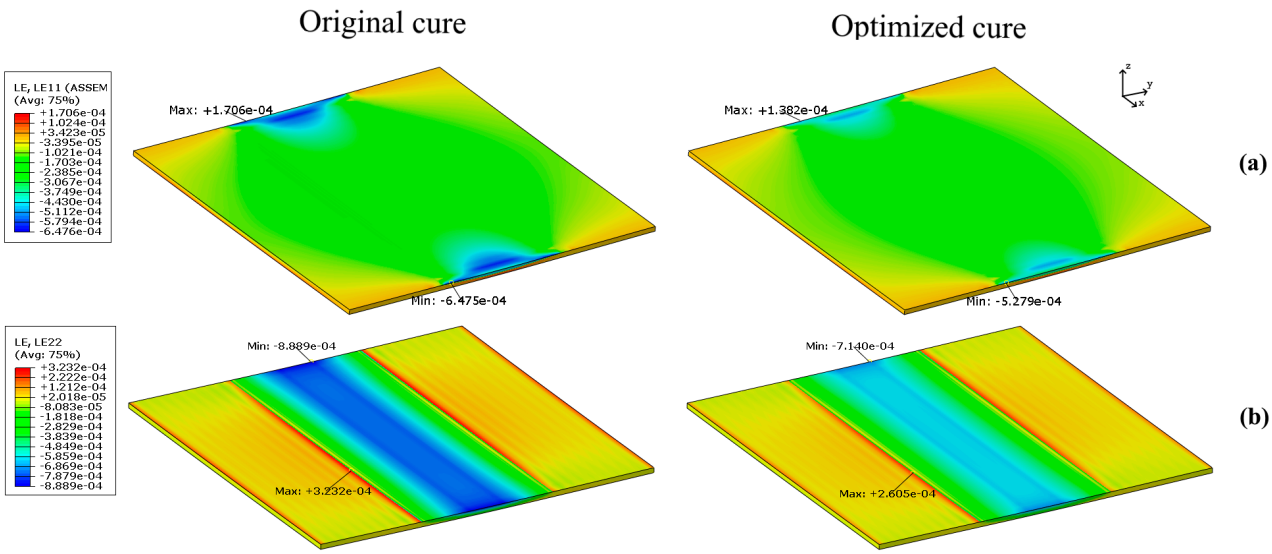

Figure 6: Results of the cure simulation on the twill weave HTA40 RM3000 scarf repair in a 300x300 mm UD IM7-CYCOM-5250-4 laminate using both the original and the optimized cure cycle, displaying results of the in-plane strains along (a) the 0°/x-direction and (b) the 90°/y-direction

Table 3: Peak stress/strain components as a result of the cure of the repair patch using both the original and the optimized cure cycle

Stress/strain component		Original cure cycle	Optimized cure cycle	difference
S11	tension	4.47E+07	3.60E+07	19.46%
	compression	-5.58E+07	-4.53E+07	18.86%
S22	tension	4.39E+07	3.58E+07	18.44%
	compression	-8.55E+07	-6.91E+07	19.21%
S33	tension	9.87E+06	7.27E+06	26.32%
	compression	-9.78E+06	-7.09E+06	27.50%
S13	tension	9.94E+06	7.78E+06	21.70%
	compression	-9.94E+06	-7.78E+06	21.69%
S23	tension	8.83E+06	6.92E+06	21.55%
	compression	-8.83E+06	-6.92E+06	21.55%
LE11	tension	1.71E-04	1.38E-04	18.99%
	compression	-6.48E-04	-5.28E-04	18.47%
LE22	tension	3.23E-04	2.61E-04	19.40%
	compression	-8.89E-04	-7.14E-04	19.68%

4 Wingbox Repair

Finally the numerical framework for repair simulation is applied to a repair of a generic wing box. The wing box consists of two 500 x 800 x 4.256 mm composite skins of IM7-CYCOM 5250-4 UD prepreg material fixed by 800 x 85 x 27.5 mm aluminium C-spars. The connection between the 2.5 mm thick C-spars and the skins is made by 26 titanium rivets per connecting surface. At the centre of the top skin, material is removed to accommodate a scarf repair to half the depth of the parent material with a ratio of 1/20 and an outer diameter of 153 mm. This material is replaced by uncured repair plies consisting of twill weave HTA-40 RM3000 plies. The parent material has a layup of $[45,0,-45,90]_{4,s}$. The plies of the repair patch are oriented with the same layup as the parent material. The ply stiffness properties of the repair patch are increased to compensate for the thickness reduction to achieve a similar structural stiffness as the actual repair patch and parent material.

4.1 Model Setup

Figure 6 displays the finite element model of the wing box including the scarf repair. The aluminium spars and the elements in the vicinity of the repair patch are modelled using quadratic hexahedral elements. To limit the computational cost of the model the bottom skin and the elements in the upper skin that are at sufficient distance from the repair patch are meshed with linear hexahedral elements. The plies in the repaired laminate are meshed individually with 1 element over the ply thickness.

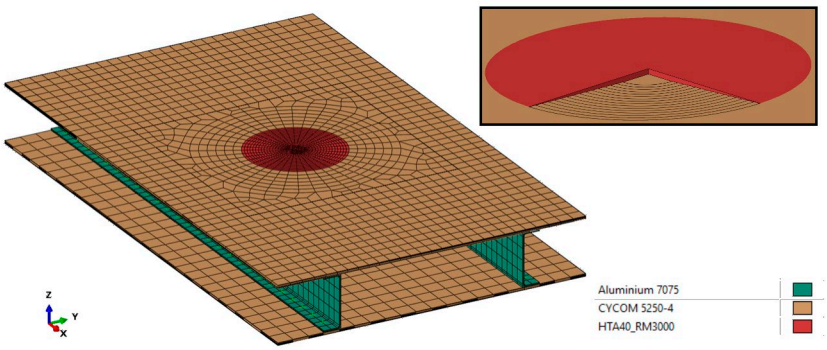

Figure 7: Finite element model of the wing box repair, displaying the aluminium spars, the CYCOM 5250-4 skins and the HTA40 RM3000 repair patch with a close up of ¾ of the patch showing the scarf angle

In contrast with the simple 1D scarf repair, the wing box repair is heated locally by the heating blanket resulting in an inhomogeneous temperature distribution. To obtain this temperature distribution a thermal analysis is performed. Figure 7 shows a basic repair set-up for the generic wing box as modelled in this section. In the thermal simulation heat is applied to the top skin over a diameter of 300 mm centred around the repair patch. As the heating blanket is temperature controlled, it is assumed that the area below the blanket follows the applied temperature cycle. Isolated boundaries are used for the rest of the top skin, as it is isolated by breather material and the vacuum bag, and the edges of the bottom skin resting on the wooden blocks. The conduction from the composite skin to the aluminium spars is assumed to be perfect, ignoring effects of gap conductance and conduction through the titanium fasteners. Convective and radiative boundary conditions are applied to all other outer surfaces of the wing box based on Moser [25]. Furthermore, open cavity radiation is defined at the inside of the wing box assuming an emissivity of 0.95 for the laminates and 0.1 for the aluminium spars.

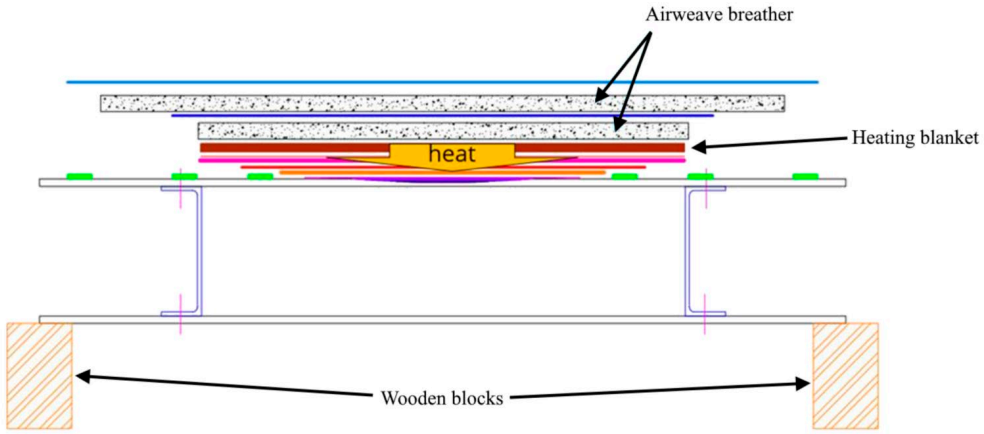

Figure 8: The repair setup for repair of the modelled wing box

The temperature profile obtained in the thermal analysis is given as load in the structural analysis. Furthermore, this temperature is used in the cure kinetics model to determine the cure induced strains and residual stresses. As the wing box is free to deform, boundary conditions are only applied to three corners of the bottom skin to prevent rigid body motions. The rivet connections between the composite skins and the aluminium spars are modelled by fixing the elements in the spars and the skins located in a small radius around the rivet to each other.

4.2 Results and Discussion

Figure 9 displays the max principal stress in the generic wing box and the out of plane stresses in the repair patch after cure. Similarly to the repair in the simple laminate, the peak residual stresses occur at the interface between the repair and the parent material. It is observed that the peak stresses are almost double the peak stresses in the simple laminate. Furthermore, with a significant out of plane normal stress of 62 MPa, there is a significant possibility of peeling of the repair patch. Compared to the rectangular repair patch, the out of plane stress components are 4-6 times higher. This increase in residual stress could be caused by the significant reduction in deformation freedom of the repair patch, as it is now surrounded by parent material, which is further constrained by the C-spars.
Table 4 gives an overview of stress and strain components with peak tensile and compressive values. It is observed that by implementing the optimized cure cycle, the out of plane normal and shear stresses could be reduced by 17-26%, strongly reducing the risk of peeling of the repair. It should be noted that the staircase geometry of the repair patch as implemented in the model causes localized peak stresses, which in the actual repair would be distributed more evenly by resin pockets in these locations. Therefore the out of plane stresses in the actual repair might well be less extreme. However, the effect of the optimized cure cycle on the residual stress remains.
Finally, it is also observed that due to the strains in the repair patch, the connections between the skins and the spars are loaded, resulting in additional stresses in the rivet connections.

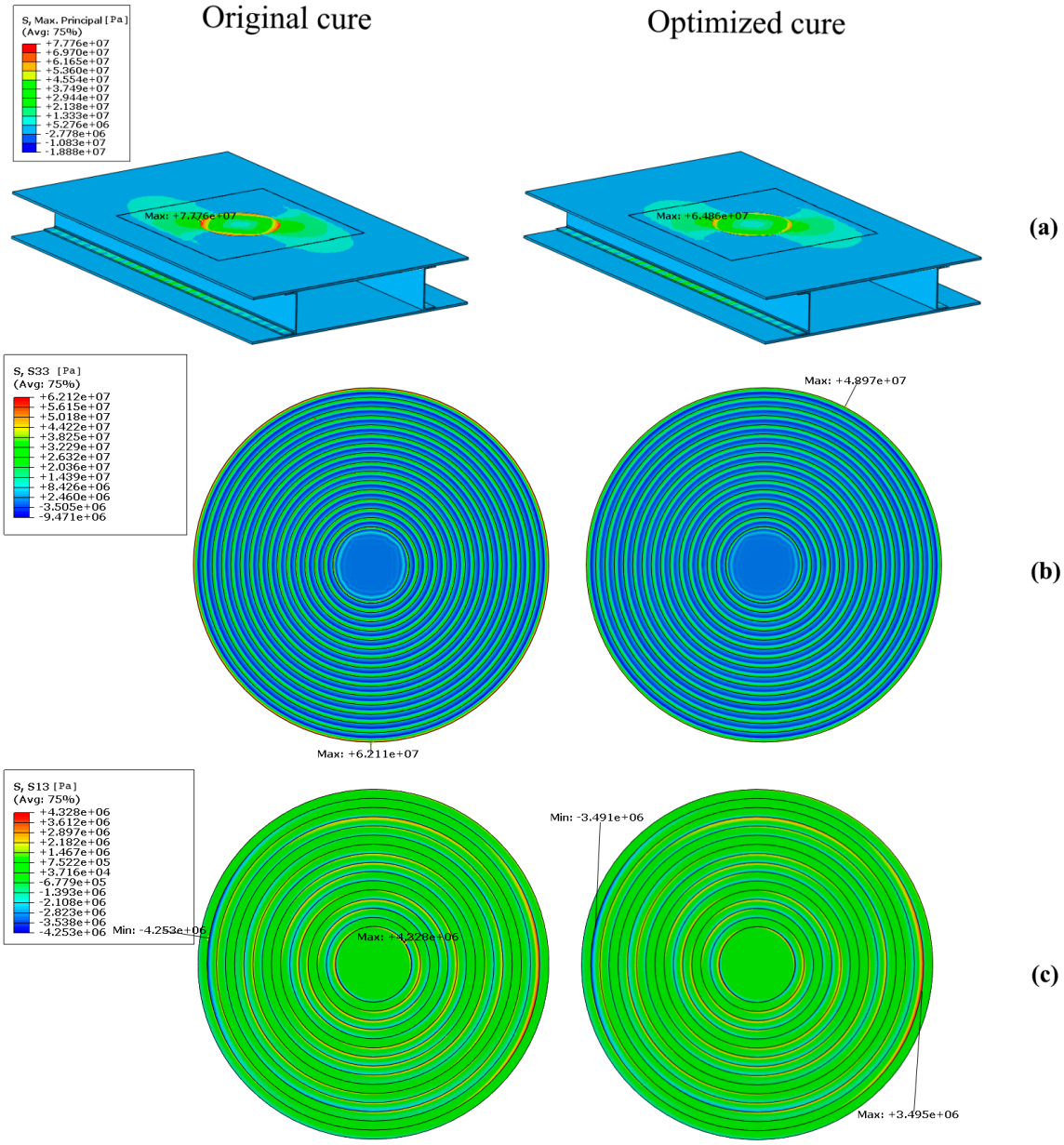

Figure 9: Results of the original and optimized cure cycle simulation on the twill weave HTA40 RM3000 scarf repair in the IM7-CYCOM-5250-4 skin of a generic wing box with (a) the max principal stresses, (b) the out of plane normal stress and (c) the out of plane shear stress with the largest components in the repair patch after cure

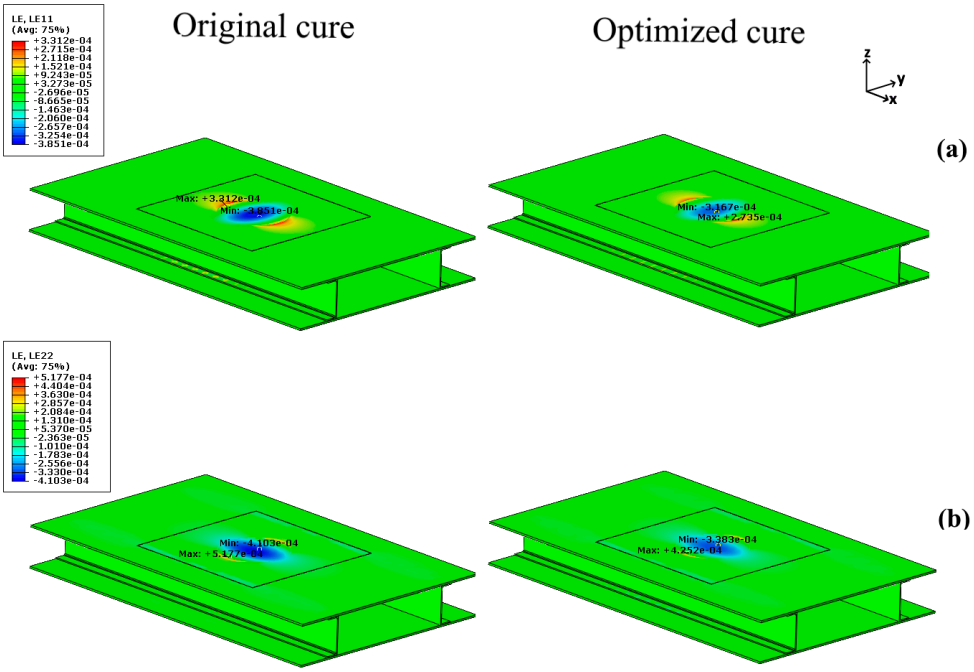

Figure 10: Results of the original and optimized cure cycle simulation on the twill weave HTA40 RM3000 scarf repair in the IM7-CYCOM-5250-4 skin of a generic wing box with (a) the in-plane strain along the length of the skin (0°/x-direction) and (b) the in-plane strain along the width of the skin (90°/y-direction) after cure

Figure 10 displays the results for the in plane strain after curing of the repair patch in the generic wing box. The largest tensile strains are observed at the connection between the patch and the parent material. In the centre of the repair patch, the compressive strains due to chemical shrinkage and cooling of the repair patch are the most significant. It is observed that the tensile strains in the y-direction Figure 10 (b) are more than 50% higher compared to the strains along the x-direction Figure 10 (a). This is mainly due to proximity of the C-spars constraining deformation of the repair patch along the y-direction. Similarly to the residual stresses, the in-plane strains are also significantly reduced by the use of the optimized cure cycle, where all in-plane strain components are reduced by approximately 17.5%.

Table 4: Peak stress/strain components as a result of the cure of the repair patch in the generic wingbox using both the original and the optimized cure cycle

Stress/strain component		Original cure cycle	Optimized cure cycle	difference
S11	tension	6.70E+07	5.58E+07	16.74%
	compression	-5.11E+07	-4.06E+07	20.49%
S22	tension	6.58E+07	5.48E+07	16.80%
	compression	-5.39E+07	-4.31E+07	20.12%
S33	tension	6.21E+07	4.90E+07	21.13%
	compression	-4.36E+07	-3.21E+07	26.46%
S13	tension	4.37E+06	3.60E+06	17.62%
	compression	-4.37E+06	-3.60E+06	17.61%
S23	tension	4.23E+06	3.45E+06	18.39%
	compression	-4.54E+06	-3.45E+06	24.10%
LE11	tension	3.31E-04	2.74E-04	17.42%
	compression	-3.85E-04	-3.17E-04	17.76%
LE22	tension	5.18E-04	4.25E-04	17.87%
	compression	-4.10E-04	-3.38E-04	17.55%

As stated before, the reduction in process induced stresses and strains strongly depends on the accuracy of the cure modelling, the used material parameters as well as the predicted temperatures. A large contributing factor in the strain reduction is the moment of gelation. As observed during the optimization of the cure cycle, it is preferred to cross the gelation point before the second temperature ramp to limit process induced strains. In the numerical simulations, this moment is strongly dependent on the cure kinetics, degree of cure at gelation and predicted temperatures, where small changes in these parameters can significantly limit the effect of the optimized cure cycle. However, even without accurate resin characterization and temperature prediction insights gained in this study could still be valuable. If during the actual curing of a repair the gelation point can be detected, this could be used as a trigger to ramp to the second dwell temperature, effectively reproducing the working principles behind the optimized cure cycle.

Besides the cure characterization, the obtained results are also strongly dependent on the used ply properties, such as the chemical shrinkage and thermal expansion coefficients. Full characterization of the materials can be a laborious and expensive process which can strongly limit the accuracy of the virtual manufacturing of composite materials. In the current study, a calibrated value for the thermal expansion and chemical shrinkage from previous research is used [12]. This calibration method significantly reduces the required experimental effort, but should be validated for the current repair set-up. Therefore, further experimental validation of the employed models is required.

5 Conclusions

Cure kinetic modelling combined with parametrization of the cure cycle can quickly give insights in the effects of different cure cycles, and how to perform an optimal cure cycle to strongly reduce process induced residual stresses The optimal cure cycle was first tested numerically on a simple scarf repair showing a significant reduction in the process induced strain of up to 20%. Furthermore, stresses along the edges of the repair were reduced by a similar amount. However, in this repair geometry, the out of plane stresses were not significant, therefore using the original cure cycle would already have a low risk of peeling of the repair.
Finally, the framework is successfully applied to a model representing a generic wingbox, showing the effectiveness of the optimized cure cycle while taking into account the underlying structures. For this geometry, the out of plane stresses were found to be significant due repair geometry and more constraining underlying structures. The optimized cure cycle reduced these out-of-plane stresses by 17-26%. This illustrates the opportunity for cure cycle optimization to strongly reduce the chance of peeling of the repair after cure. Finally, it is observed that due to the repair residual stresses are not only introduced around the repair patch, but are also in the underlying structure.

It is shown that this framework with optimisation of the cure cycle can support the patch fabrication with accurate design and analysis for repairs with minimum distortion. However, further experimental validation of the modelling approach is required.

6 Acknowledgements

The research presented in this paper has been performed in the scope of the Defence Technology Project “Composite infusion repair assisted by process simulation” funded by the Dutch Ministry of Defence, Defence order number *4501255425 NTP 17-21*. The authors are grateful to John Bronder of the Dutch Ministry of Defence for the contributions and feedback to the research described in this paper.

7 References

[1] A. A. Johnston, An integrated model of the development of process-induced deformation in autoclave processing of composite structures, Vanvouver: The University of British Columbia, 1997.

[2] S. Wijskamp, Shape distortions in composites forming, Enschede: Universiteit Twente, 2005.

[3] T. Garstka, Separation of process induced distortions in curved composite laminates, Bristol: University of Bristol, 2005.

[4] J. M. Svanberg, Predictions of Manufacturing Induced Shape Distortions, Luleå: Luleå University of Technology, 2002.

[5] M. W. Nielsen, Prediction of process induced shape distortions and residual stresses in large fibre reinforced composite laminates, Copenhagen: Technical University of Denmark, 2012.

[6] K. VanClooster, J. Gilbert, F. Pascon en L. V. Stepan, „Predicting the Influence of Manufacturing Parameters on Curing Generated Deformations Using Thermo-mechanical Modelling," in *American Society for Composites*, Seattle, 2018.

[7] V. Chabridon, „Robust Probabilistic Analyses of Composite Part Manufacturing," National Aerospace Laboratory NLR, Amsterdam, 2014.

[8] M. Ridha, V. B. Tan en T. E. Tay, „Traction-separation laws for progressive failure of bonded scar repair of composite panel," *Composite structures,* vol. 93, nr. 4, pp. 1239-1245, 2011.

[9] P. G. Slattery, C. T. McCarthy en R. M. O'Higgings, „Assessment of residual strength of repaired solid laminate composite materials through mechanical testing," *Composite Structures,* vol. 147, pp. 122-130, 2016.

[10] M. Hautier, D. Lévêque, C. Huchette en P. Olivier, „Investigation of composite repair method by liquid resin infiltration," *Plastics, Rubber and Composites,* vol. 39, nr. 3-5, pp. 200-207, 2010.

[11] A. Kondratiev, V. Pistek, L. Smovziuk, M. Shevtsova, A. Fomina, P. Kučera en A. Prokop, „Effects of the Temperature-Time Regime of Curing of Composite Patch on Repair Process Efficiency," *Polymers,* vol. 13, p. 4342, 2021.

[12] T. Koenis, N. v. Hoorn en W. v. d. Brink, „Calibration and Validation of a Numerical Curing Model Using AS4/8552 Asymmetric Laminated Composite Plates," in *Presentations to VIII Conference on Mechanical Response of Composites*, Gothenburg, 2021.

[13] M. R. Kamal en S. Sourour, „Kinetics and thermal characterization of thermoset cure," *Polym Eng Sci,* vol. 13, pp. 59-64, 1973.

[14] G. Struzziero, B. Remy en A. A. Skordos, „Measurement of thermal conductivity of epoxy resins during cure," *Journal of Applied Polymer science,* vol. 136, p. 47015, 2019.

[15] N. Pantelelis, E. Bistekos, W. Gerrits, S. Wilkens, D. Breen en S. Wilson, „Non-intrusive intelligent cure monitoring for enhancing the manufacturing of high-temp composite structures," in *SAMPE Europe Conference 2021*, Baden/Zürich, 2021.

[16] J. Gao, L. Li, Y. Deng, Z. Gao, C. Xu en Z. Mingxi, „Study of gelation using Differential Scanning Calorimetry (DSC)," *Journal of Thermal Analysis,* vol. 49, pp. 303-310, 1997.

[17] N. Zobeiry en A. Poursartip, „The origins of residual stress and its evaluation in composite materials," *Structural Interity and Durability of Advanced Composites,* pp. 43-72, 2015.

[18] C. C. Chamis, *NASA Tech. Memo 8329,* 1983.

[19] C. C. Chamis, F. Abdi, M. Garg, L. Minnetyan, H. Baid, D. Huang, J. Housner en F. Talagani, „Micromechanics-based progressive failure analysis prediction for WWFE-III composite coupon test cases," *Journal of Composite Materials,* vol. 47, nr. 20, pp. 2695-2712, 2013.

[20] N. van Hoorn, C. Kassapoglou en W. M. van den Brink, „Impact repsonse prediction and sensitivity analysis of thick laminated composite plates," Royal NLR, Amsterdam, 2020.

[21] T. Ishikawa en T.-W. Chou, „In-Plane Thermal Expansion and Thermal Bending Coefficients of Fabric Composites," *Journal of Composite Materials,* vol. 17, nr. 2, pp. 92-104, 1983.

[22] A. Saltelli, P. Annoni, I. Azzini, F. Campolongo, M. Ratto en S. Tarantola, „Variance based sensitivity analysis of model output. Design and estimato for the total sensitivity index," *Computer Physics Communications,* vol. 181, nr. 2, pp. 259-270, 2010.

[23] I. M. Sobol, „Global sensitivity indices for nonlinear mathematical models and their Monte Carlo estimates," *Mathematics and Computers in Simulation,* vol. 55, nr. 1-3, pp. 271-280, 2001.

[24] C. E. Materials, *Cycom 5250-4 Prepreg System Technical Data Sheet,* 2011.

[25] L. Moser, Experimental Analysis and Modeling of Susceptorless Induction Welding of High Performance Thermoplastic Polymer Composites, Kaiserslautern: Technische Universität Kaiserslautern, 2012.

Dedicated to innovation in aerospace

Royal NLR - Netherlands Aerospace Centre

NLR operates as an objective and independent research centre, working with its partners towards a better world tomorrow. As part of that, NLR offers innovative solutions and technical expertise, creating a strong competitive position for the commercial sector.

NLR has been a centre of expertise for over a century now, with a deep-seated desire to keep innovating. It is an organisation that works to achieve sustainable, safe, efficient and effective aerospace operations.
The combination of in-depth insights into customers' needs, multidisciplinary expertise and state-of-the-art research facilities makes rapid innovation possible. Both domestically and abroad, NLR plays a pivotal role between science, the commercial sector and governmental authorities, bridging the gap between fundamental research and practical applications. Additionally, NLR is one of the large technological institutes (GTIs) that have been collaborating over a decade in the Netherlands on applied research united in the TO2 federation.

From its main offices in Amsterdam and Marknesse plus two satellite offices, NLR helps to create a safe and sustainable society. It works with partners on numerous programmes in both civil aviation and defence, including work on complex composite structures for commercial aircraft and on goal-oriented use of the F-35 fighter. Additionally, NLR helps to achieve both Dutch and European goals and climate objectives in line with the Luchtvaartnota (Aviation Policy Document), the European Green Deal and Flightpath 2050, and by participating in programs such as Clean Sky and SESAR.

For more information visit: **www.nlr.org**

Postal address
PO Box 90502
1006 BM Amsterdam, The Netherlands
e) info@nlr.nl **i)** www.nlr.org

Royal NLR
Anthony Fokkerweg 2
1059 CM Amsterdam, The Netherlands
p) +31 88 511 3113

Voorsterweg 31
8316 PR Marknesse, The Netherlands
p) +31 88 511 4444